Mod Pathol 36 (2023) 100039

MODERN PATHOLOGY

USCAP UNITED STATES AND CANADIAN ACADEMY OF PATHOLOGY
Creating a Better Pathologist

Journal homepage: https://modernpathology.org/

Research Article

Pediatric *BCOR*-Altered Tumors From Soft Tissue/Kidney Display Specific DNA Methylation Profiles

Claudia M. Salgado[a], Rita Alaggio[b,*], Andrea Ciolfi[c], Angelica Zin[d], Francesca Diomedi Camassei[b], Lucia Pedace[e], Giuseppe Maria Milano[e], Annalisa Serra[e], Angela Di Giannatale[e], Angela Mastronuzzi[e], Andrea Gianatti[f], Gianni Bisogno[g], Andrea Ferrari[h], Marco Tartaglia[c], Miguel Reyes-Múgica[a], Franco Locatelli[e,i], Evelina Miele[e,*]

[a] *Division of Pathology, University of Pittsburgh Medical Center Children's Hospital of Pittsburgh, Pittsburgh, Pennsylvania;* [b] *Pathology Unit, Bambino Gesù Children's Hospital, Istituto di Ricovero e Cura a Carattere Scientifico, Rome, Italy;* [c] *Genetics and Rare Diseases Research Division, Bambino Gesù Children's Hospital, Istituto di Ricovero e Cura a Carattere Scientifico, Rome, Italy;* [d] *Clinica di Oncoematologia Pediatrica Azienda Ospedaliera, Università di Padova, Padova, Italy;* [e] *Department of Pediatric Onco-Hematology and Cell and Gene Therapy, Bambino Gesù Children's Hospital, Istituto di Ricovero e Cura a Carattere Scientifico, Rome, Italy;* [f] *Department of Pathology, Azienda Socio Sanitaria Territoriale Papa Giovanni XXIII, Bergamo, Italy;* [g] *Department of Pediatric Hematology-Oncology, Università di Padova, Padova, Italy;* [h] *Pediatric Oncology Unit, Medical Oncology and Hematology Department, Fondazione Istituto di Ricovero e Cura a Carattere Scientifico Istituto Nazionale Tumori, Milano, Italy;* [i] *Catholic University of the Sacred Heart, Rome, Italy*

ARTICLE INFO

Article history:
Received 27 September 2022
Accepted 3 October 2022
Available online 10 January 2023

Keywords:
BCOR
diagnosis
DNA methylation
pediatric sarcoma
survival

ABSTRACT

In the pediatric population, BCL6-correpresor gene (*BCOR*)—upregulated tumors include primitive myxoid mesenchymal tumors/undifferentiated sarcomas (PMMTI/UND), clear cell sarcomas of the kidney (CCSK), and high-grade neuroepithelial tumors (HG-NET). We investigated DNA methylation (DNAm) and copy number variation (CNV) profiling in these tumors (N = 34) using an Illumina EPIC BeadChip to better define the potential use of these tools to confirm diagnosis and predict outcomes. Twenty-seven tumors from 25 patients (age range, 0-10 years), showed molecular confirmation of genetic abnormalities as follows: *BCOR* internal tandem duplication in 14 PMMTI/UND, 8 CCSK, and 3 HG-NET and *YWHAE* fusions in 2 PMMTI/UND. The remaining 7 cases lacking informative molecular data were analyzed by immunophenotyping and were included in the study as a training cohort, clearly separated from the main study group. These were 4 PMMTI, 1 HG-NET, and 1 CCSK in which poor RNA preservation precluded the confirmation of *BCOR* rearrangements and 1 CCSK in which no rearrangements were found. DNAm data were compared with those of brain tumor and/or sarcoma classifier. Differentially methylated regions (DMRs) were analyzed in the 3 groups. Twenty-two cases of the 24 molecularly confirmed PMMTI/UND and CCSK and 3 of 6 of those with only immunophenotyping were classified within the methylation class "*BCOR*-altered sarcoma family" with optimal calibrated scores. PMMTI/UND and CCSK showed similar methylation profiles, whereas thousands of DMRs and significantly enriched pathways were evident between soft tissue/kidney tumors and HG-NET. The CNV analysis showed an overall flat profile in 19 of the 31 evaluable tumors (8/10 CCSK; 9/18 PMMTI/UND; 2/4 HG-NET). The most frequent CNVs were 1q gain and 9p and 10q loss. Follow-up time data were available for 20 patients: ≥2 CNV significantly correlated with a worse overall survival rate. In conclusion, soft tissue and kidney *BCOR* sarcomas matched with *BCOR*-altered sarcoma methylation class, whereas those from the brain matched with the central nervous system tumor classifier HG-NET BCOR, supporting the notion that DNAm profiling is an informative diagnostic tool. CNV alterations were associated with a more aggressive clinical behavior.

Introduction

The BCL6-correpresor gene (*BCOR*) is located on chromosome Xp11.4 and has 16 alternatively spliced exons, resulting in several

These authors contributed equally: Claudia M. Salgado and Rita Alaggio.
These authors contributed equally: Franco Locatelli and Evelina Miele.
* Corresponding author.
E-mail addresses: rita.alaggio@opbg.net (R. Alaggio), evelina.miele@opbg.net (E. Miele).

https://doi.org/10.1016/j.modpat.2022.100039

protein isoforms.[1] The principal isoform is a ubiquitously expressed transcriptional repressor. Two domains—B-cell lymphoma 6 (BCL6) and PUFD-binding—primarily mediate the function of *BCOR*.[1] Among these, the PUFD-binding domain is the site that mediates BCOR binding to the noncanonical polycomb repressive complex 1, which marks histones for recruitment.[2] Through this mechanism, BCOR regulates the expression of genes involved in early embryonic development, mesenchymal stem cell function, and hematopoiesis. In cancer, major groups of *BCOR* alterations include *BCOR* gene fusions and an internal tandem duplication of the PUFD domain, called *BCOR-ITD*.[1]

In the pediatric population, *BCOR*-upregulated tumors, which include tumors with *BCOR* gene alterations and *YWHAE* fusions, were initially described in clear cell sarcoma of kidney (CCSK), in which these alterations occur in approximately 85% of the cases.[3] In 2016, the same genetic alteration was described in a subgroup of undifferentiated infantile soft tissue tumors, including primitive myxoid mesenchymal tumors of infancy (PMMTI) and undifferentiated round cell sarcoma (UND)[4] and in a subset of high-grade neuroepithelial tumors (HG-NETs) in the central nervous system (CNS).[5] The same genetic alteration has been reported in the adult-onset endometrial stromal sarcoma of high grade (ESS-HG).[6] All these tumors share a similar histology and transcriptional signature that includes the overexpression of BCOR, cyclin D1, and BCL6.

In cancer cells, transcriptional changes can be driven by genetic and/or epigenetic alterations. DNA methylation (DNAm) is an epigenetic process that can modify gene expression without altering the DNA sequence. During tumorigenesis, changes in the DNAm pattern, with hypomethylation of non-CpG islands and hypermethylation of CpG islands, lead to abnormal silencing of several genes, including many tumor suppressor genes.[7] These changes in DNAm of tumor cells are relatively stable during the course of disease and represent a combination of those characterizing the cell of origin and those somatically acquired in the tumor cells.[7]

Recently, several efforts to examine the cancer methylome using genome-wide techniques have contributed to the generation of a large database of methylation profiles of many tumor types. These profiles can be used in tumor classification, allowing, among other uses, stratification of cancer subtypes and prediction of cancer outcomes. DNAm profiling is now part of the clinical diagnostic workup in the classification of CNS tumors,[8] and its application in the classification and differential diagnosis of soft tissue sarcoma is progressively expanding.[9,10] In the group of tumors with *BCOR* alterations, 3 different methylation classes are recognized: small blue round cell tumor with *BCOR* alteration (SBRCT-BCOR), CCSK, and ESS-HG.[11] However, DNAm and CNV profiling of pediatric tumors with BCOR overexpression, including *BCOR-ITD* and *YWHAE* fusions, have not been investigated in depth. This study aimed to explore DNAm and CNV profiles in pediatric tumors with *BCOR-ITD* or *YWHAE* fusions to better define their potential contribution to the diagnostic confirmation and stratification, as well as their prognosis prediction value in these tumors, and to compare the epigenetic variations of these 3 *BCOR*-related pediatric tumors.

Materials and Methods

Sample Collection

Institutional and consultation files from 2 large pediatric institutions (Bambino Gesù Children's Hospital, Italy, and UPMC Children's Hospital of Pittsburgh, Pennsylvania) were queried. All tumors with a histologic diagnosis of PMMTI/UND, CCSK, and HG-NET were selected for a histologic review. Ten of the PMMTI/UND were included in a previous study.[12]

Pathology reports and samples, including hematoxylin and eosin–stained slides, immunohistochemical studies, and formalin-fixed paraffin-embedded (FFPE) tissue of tumor samples from each case, were retrieved. An expert pathology review was performed by experienced pathologists (R.A., C.M.S., M.R.-M.). The presence of characteristic histologic and immunohistochemical features with strong and diffuse nuclear positive immunohistochemical staining for BCOR, BCL6, and cyclinD1 was considered supportive of the diagnosis in cases with poorly preserved material for molecular characterization. Pertinent clinical information was obtained from electronic medical records and available consultation material.

A molecular analysis for the detection of *BCOR-ITD* and *YWHAE* fusions by RT-PCR was performed in cases not already characterized at the time of diagnosis.

All cases underwent methylation profiling. In samples with failure of molecular characterization because of technical problems, methylation data were compared with those of molecularly confirmed tumors with *BCOR-ITD* to obtain a final integrated diagnosis according to the methylation clustering.

For the hierarchical clustering and multidimensional scaling analysis (MDS), we used a cohort of 26 the previously published HG-NET BCOR[13] as a control group and samples of mimics randomly extracted from internal and external data sets[13] among those classifying as Ewing sarcoma (EWS) (n = 13), CIC-rearranged sarcoma (EFT-CIC) (n = 8), atypical teratoid rhabdoid tumors (ATRT) (n = 15), and rhabdoid tumors (n = 2).

Detection of BCOR-ITD

RNA was extracted from 4-μm FFPE sections using the Absolutely RNA FFPE Kit (Agilent). One microgram of RNA was retrotranscribed to cDNA with EuroScript M-MLV Reverse Transcriptase (RNase H-; Euroclone). PCR amplification was performed using the BIOTAQ DNA Polymerase (Bioline) according to the manufacturer's instructions. The PCR reaction mixture contained 1.5 mM of $MgCl_2$, 0.2 μM of forward (`5'-GACCTGGAAGCCTTCAACCC-3'`) and reverse (`5'-GTACATGGTGGGTCCAGCTTG-3'`) primers, 1× PCR buffer, 0.4 mM of each dNTPs, 0.5 U of Taq polymerase, and 1 μL of the RT product in a final 20-μL reaction volume. The RNA quality and efficiency of reverse transcription were assessed by analyzing the expression of *B2M* and *GAPDH*. PCR reaction products were electrophoresed through 2% agarose gels, and their sizes were determined by a comparative analysis with DNA Marker VI (Roche).

DNAm Analysis

DNAm profiling was assessed as previously described.[14,15] Tumor areas with the highest tumor cell content (≥70%) were selected for the analysis. DNA was extracted according to MagPurix FFPE DNA Extraction Kit (Zzinexts) for the automatic extraction of genomic DNA. Samples were analyzed using Illumina Infinium Human Methylation EPIC Beadchip arrays (Illumina),

Table 1
Clinicopathologic findings, treatment, and follow-up of the pediatric *BCOR*-upregulated tumors with and without molecular confirmation

Case	Age (y)	Sex	Location	Treatment	Recurrence/metastasis	Follow-up (y)
Molecularly confirmed						
1ST	0.5	M	Paravertebral	NA	NA	NA
2ST	10 (Recurrence)	F	Paraspinal gluteal soft tissue	S	Recurrence (of case 14)	DOD (1 from the relapse)
3ST	1	M	Head extradural	NA	NA	PD
4ST	0	F	Sacrococcygeal	C+S	Yes (3 recurrence)	DOD (2.2)
5ST	0.8	F	Back	NA	NA	NA
6ST	0.5	F	Orbital	NA	NA	DOD
7ST	0	M	Upper leg (limbs)	C+S	Yes (4 recurrences)	Alive (17)
8ST	0.3	M	Larynx	S+C	Yes (6 recurrence)	DOD (2)
9ST	0	M	Paraspinal	NA	NA	Recent
10ST	0.2	M	Thorax	C	No	DOD (0.3)
11ST	0.3	F	Paraspinal-thorax	S+C	No	Alive (5)
12ST	0.2	F	Jaw	C+R+S	No	DOD (0.7)
13ST	0.5	M	Thorax	C	Yes (1 recurrence)	DOD (1.1)
14ST	0.2	F	Paraspinal gluteal soft tissue	S+C	Yes (1 recurrence)	DOD (relapse after 10)
15ST	0.4	M	Pelvis	S+C+S	Yes (3 recurrence)	DOD (2.5)
16ST	4	M	NA	NA	NA	Recent
1N	1.2	M	Cerebellum	GTR/C	relapsed	PD (0.25)
2N	1.5	M	Cerebellum	GTR/C	Third relapse	NA
3N	1.5	M	Brain	PR/C/R	Persistent lesion	DOD (1)
1K	0.2	M	Kidney	GTR/C	None	Alive (2.5)
2K	NA	M	Kidney	NA	NA	NA
3K	3	F	Kidney	GTR/C/R	None	Alive (17)
4K	2	M	Kidney	NA	NA	Alive (7.6)
5K	0.6	M	Kidney	PR/C/R	None	Alive (14)
6K	2	M	Kidney	GTR/C/R	None	Alive (4)
7K	1	M	Kidney	PR/C/R	Local relapse and bone metastasis	DOD (6)
8K	6	M	Kidney	GTR/C/R	None	Alive (1.5)
Without molecular confirmation						
17ST	0.3	F	Deep dermis/subcutaneous	NA	NA	PD
18ST	<1	M	NA	NA	NA	NA
19ST	0.2	F	Pelvis	NA	NA	DOD (0.25)
20ST	0.3	F	Orbital	S+C/R	Persistent lesion	Alive on treatment (2)
30N	NA	M	Brain	NA	NA	NA
9K	7	M	Kidney	NA	NA	DOD (0.6)
10K	5	M	Kidney	GTR/C/R	Bone metastasis	Alive (5)

C, chemotherapy; DOD, died of disease; GTR, gross total resection; NA, not available; PD, progressive disease; PR, partial resection; R, radiation therapy; S, surgery.

according to the manufacturer's instructions, on the Illumina iScan Platform (Illumina). In detail, 250-ng DNA was used as the input material.

The generated DNAm data were compared with those of the sarcoma classifier v12.2[11] and CNS tumor classifier v.11b4,[13] developed by Heidelberg University and DKFZ (https://www.molecularneuropathology.org/mnp/classifier/9, accessed March 15, 2021) to assign a subgroup score for the tumors in the recognized methylation classes and to generate the CNV plots. EPIC BeadChip data were further analyzed as previously reported[15] using R (v.4.1.2), with the ChAMP package (v.2.21.1) for quality checks and filters. Batch effects were inspected by the singular value decomposition analysis, whereas probes with detection *P* values of >.1, those located on chromosomes X and Y, those known to contain a SNP at the CpG interrogation, and those known to cross-react with multiple chromosomal locations were excluded from the analysis.[16]

The hierarchical clustering analysis was performed using the Ward hierarchical agglomerative clustering method and Euclidean distance[17] using bootstrap resampling (nboot = 1000)[18] and visualized by heatmap depicting normalized β values. MDS on the cohort samples was performed using the cmdscale function with the Euclidean distance.

Differentially methylated regions (DMRs) were identified by DMRcate (as implemented in ChAMP pipeline), using default statistical thresholds. The functional enrichment analysis of DMR promoters was performed using missMethyl package[19] to identify significantly enriched KEGG and MSigDB pathways.

High-density DNAm arrays allowed for determining CNVs that were generated for the reported case, as described.[13] The integrative genomic viewer was used for graphical visualization of structural rearrangements and mapping genes onto regions of interest.

Survival Analysis

The Kaplan-Meier method was used to estimate overall survival (OS) probabilities; differences between the groups were compared using the log-rank test. Hazard ratio for death was calculated using 95% CI. Patients whose follow-up time was unavailable were excluded from the analyses. Graph generation and statistical analyses were performed using the Prism software (v.6.0; GraphPad).

Table 2
Morphologic and molecular features of the pediatric *BCOR*-upregulated tumors with and without molecular confirmation

Case	Histology	Genetic	Idat	Sarcoma class/CNS class for HG-NET	Calculated score	CNV
Molecularly confirmed						
1ST	PMMTI	*BCOR-ITD*	203724130099_R01C01	SBRCT-BCOR	0.99	Flat
2ST	PMMTI	*BCOR-ITD*	203724130138_R03C01	SBRCT-BCOR	0.99	1q gain, 9p loss (*CDKN2A/B*), 10q loss (*PTEN*)
3ST	PMMTI	*BCOR-ITD*	203724130099_R06C01	SBRCT-BCOR	0.99	Flat
4ST	UND	*BCOR-ITD*	203724130099_R07C01	SBRCT-BCOR	0.99	CDK6 amplification
5ST	PMMTI	*BCOR-ITD*	203724130099_R08C01	SBRCT-BCOR	0.99	1q gain
6ST	PMMTI	*BCOR-ITD*	203724130150_R06C01	SBRCT-BCOR	0.99	Flat
7ST	PMMTI	*BCOR-ITD*	204076520057_R08C01	CCSK	0.98	Flat
8ST	PMMTI	*BCOR-ITD*	203923030008_R04C01	SBRCT-BCOR	0.99	10 loss (*PTEN*), 3p gain
9ST	PMMTI	*YWHAE::NUTM2*	204094670160_R01C01	ESS-HG	0.99	Partial gain 10q
10ST	UND	*BCOR-ITD*	204076520057_R01C01	SBRCT-BCOR	0.92	NE
11ST	UND	*YWHAE::NUTM2*	204237140045_R05C01	ESS-HG	0.77	19p single region loss, 20q loss, 21q loss
12ST	UND	*BCOR-ITD*	204237140045_R06C01	SBRCT-BCOR	0.99	Flat
13ST	PMMTI	*BCOR-ITD*	204237140045_R07C01	SBRCT-BCOR	0.99	Flat
14ST	PMMTI	*BCOR-ITD*	205537620098_R01C01	SBRCT-BCOR	0.99	Flat
15ST	PMMTI	*BCOR-ITD*	205537620098_R02C01	SBRCT-BCOR	0.99	Flat
16ST	PMMTI	*BCOR-ITD*	205617070024_R04C01	ESS-HG	0.98	9p loss (*CDKN2A/B*)
1N	HG-NET	*BCOR-ITD*	201496710180_R06C01	HG-NET BCOR	0.9	Flat
2N	HG-NET(r)	*BCOR-ITD*	201496710180_R08C01	HG-NET BCOR	0.99	Deletion at telomerase region of several chromosomes
3N	HG-NET(r)	*BCOR-ITD*	204234160159_R01C01	HG-NET BCOR	0.95	1p loss, 1q gain, 2q partial gain, 3p pericentromeric loss, 4p partial gain, 7 gain, 13q loss (*RB1*), 18q loss
1K	CCSK	*BCOR-ITD*	203939360062_R03C01	SBRCT-BCOR	0.99	Flat
2K	CCSK	*BCOR-ITD*	203939360062_R05C01	SBRCT-BCOR	0.99	Flat
3K	CCSK	*BCOR-ITD*	203939360069_R01C01	SBRCT-BCOR	0.99	Flat
4K	CCSK	*BCOR-ITD*	203923030008_R03C01	CCSK	0.99	Flat
5K	CCSK	*BCOR-ITD*	204234160159_R02C01	CCSK	0.99	Flat (gain of single gene on 10p)
6K	CCSK	*BCOR-ITD*	204234160159_R05C01	SBRCT-BCOR	0.77	Flat
7K	CCSK	*BCOR-ITD*	204234160159_R06C01	CCSK	0.99	Flat
8K	CCSK	*BCOR-ITD*	204339390059_R01C01	SBRCT-BCOR	0.99	1q gain, 10q loss
Without molecular confirmation						
17ST	PMMTI	NA	203724130099_R04C01	ESS-HG	0.99	NE
18ST	PMMTI	NA	203724130099_R05C01	ESS-HG	0.81	NE
19ST	PMMTI	NA	204776850091_R03C01	ESS-HG	0.5	Partial gain 10q
20ST	PMMTI	NA	204076520057_R02C01	ESS-HG	0.99	Flat
30N	HG-NET	NA	202172220170_R04C01	HG-NET BCOR	0.99	Flat
9K	CCSK	NA	204094670162_R05C01	ESS-HG	0.99	1q gain, 1p loss, 9p loss (*CDKN2A/B*), 13q loss (*RB1*)
10K	CCSK	*BCOR-ITD* PCR negative	204234160159_R03C01	CCSK	0.83	Flat (loss of single region on 6q)

CCSK, clear cell sarcoma of the kidney; CNS, central nervous system; CNV, copy number variation; ESS-HG, endometrial stromal sarcoma (high grade); HG-NET, high-grade neuroepithelial tumors; NA, not available; NE, not evaluable; PMMTI, primitive myxoid mesenchymal tumors of infancy; (r), relapse; SBRCT-BCOR, small blue round cell tumor with *BCOR* alteration; UND, undifferentiated sarcoma.

Results

Clinical Findings and Molecular/Genetic Results

The study group included 27 tumors from 25 patients (age range, 0-10 years), with molecular confirmation of genetic abnormalities as follows: *BCOR-ITD* in 14 PMMTI/UND, 8 CCSK, and 3 HG-NET and *YWHAE* fusions in 2 PMMTI/UND (Tables 1 and 2). In cases 14ST and 1N, the analyses were also performed on the respective recurrent tumors, 2ST and 2N (Tables 1 and 2). We analyzed 7 additional cases lacking molecular confirmation but with surrogate immunohistochemistry (BCOR and CCND1 staining) as a training cohort. In 6 cases (4 PMMTI/UND, 1 CCSK, and 1 HG-NET), molecular characterization by RT-PCR was inconclusive because of poor RNA preservation, and in 1 CSSK case, RT-PCR screening did not reveal any known rearrangements (case 10K) (Tables 1 and 2).

Clinical characteristics and available follow-up of all cases according to molecular characterization are summarized in Table 1.

Most PMMTI/UND cases were diagnosed in the first year of life, with a median age at diagnosis of 0.4 years (range, 0-4 years, 10 years for the relapsed case 2ST) and a boy-to-girl ratio of 4:3. PMMTI/UND were identified in various anatomical sites, including the thorax and back (n = 4), paravertebral/paraspinal (n = 3), head extradural or orbital (n = 3), deep dermis (n = 2), larynx (n = 1), jaw (n = 1), sacrococcygeal (n = 1), gluteal (n = 1), and upper legs (n = 1).

CCSK occurred in older children, with a median age of 2 years (range, 0.7-7 years) and a boy-to-girl ratio of 9:1. Two of the 3 HG-NET occurred in boys younger than 1.6 years.

Follow-up data were available for 25 patients (16 PMMTI/UND, 1 HG-NET, and 8 CCSK). The average follow-up was 4 years (range, 4 months to 17 years). Nine of the 15 (60%) patients with PMMTI/

UND died of the disease, 2 are alive with disease progression, and 4 are in complete remission (2 cases have a shorter follow-up). Two of the 8 patients with CCSK (25%) and 1 of the 2 patients with HG-NET died from disease progression.

Morphologic and Immunophenotypic Findings

The predominant morphologic features of soft tissue tumors are summarized in Table 2. The histologic findings of PMMTI are previously detailed.[12,20] In brief, they show medium-sized, round-to-elongated cells with round-oval nuclei, finely dispersed chromatin, and a thin rim of amphophilic cytoplasm. Frequently, there are cytoplasmic vacuoles imparting a signet-ring–like cellular appearance and a prominent myxoid stroma with a delicate vascular network. Tumors diagnosed as UND showed similar features but denser cellularity and frequent mitoses. In some cases, there was cytologic atypia but no cellular pleomorphism or anaplasia. Morphologic features of PMMTI cases lacking molecular characterization were undistinguishable from those of molecularly confirmed ones.

CCSK appeared morphologically similar to tumors of the soft tissue with *BCOR* alterations (Fig. 1). They featured small- to medium-sized cells with pale eosinophilic to amphophilic cytoplasm, nuclei with uniformly distributed chromatin, and no nucleoli. The cells were embedded in a prominent myxoid matrix with curvilinear vessels and arranged in a trabecular or solid pattern. Two CCSK cases (9K and 10K; without molecular confirmation) were highly cellular, with prominent spindle cell morphology and minimal myxoid stroma in 1 case (9K). The mitoses were frequent in both conditions (Supplementary Fig. S1).

CNS HG-NETs showed a solid-to-fascicular pattern with focal microcystic changes. The tumors combined spindle-to-oval cells with fine chromatin and focal pseudorosettes with an ependymoma-like appearance (Fig. 2).[21]

The immunohistochemical analysis, at the time of diagnosis of all tumors, showed negative results for desmin, myogenin, SMA, S100, and pan-cytokeratin. BCOR immunostaining showed diffuse and strong nuclear staining in all cases (Fig. 1D, H). All tumors tested for cyclin D1 showed a strong and diffuse nuclear staining[22] (Supplementary Fig. S1, case 9K).

DNAm Profiling

The results of the methylation tumor class by case are tabulated in Table 2. All primary and relapsed CNS tumors were classified as HG-NET BCOR with optimal calibrated scores (>0.9) according to the CNS tumor classifier (v.11b4).

Twenty-two of the 24 molecularly confirmed PMMTI/UND and CCSK were classified in the methylation class family “sarcoma

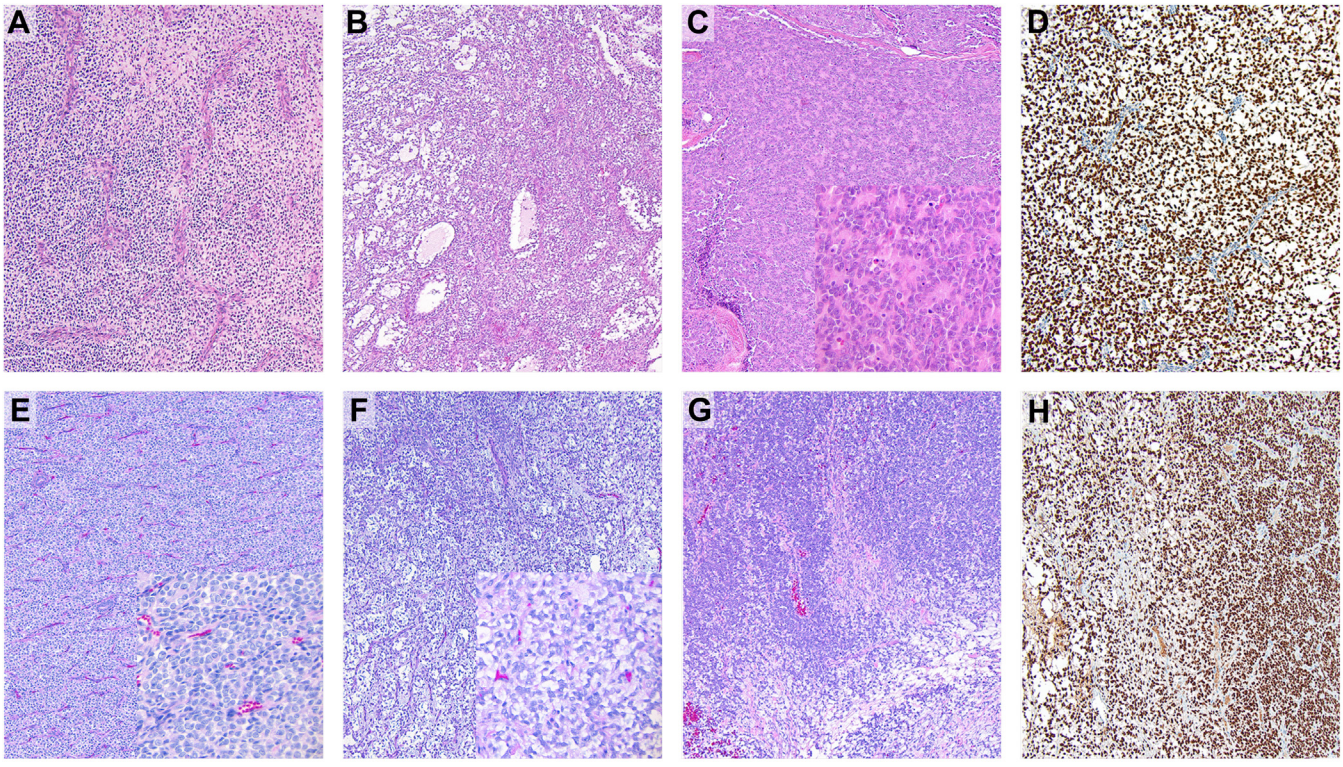

Figure 1.
Morphologic features of the primary soft tissue (A-D) and kidney tumors (E-H) with BCL6-correpresor gene (*BCOR*) alterations. (A) Soft tissue tumor showing myxoid areas with primitive round, ovoid, or spindle cells with a delicate capillary network (case 1ST). (B) Some tumors show pseudocystic areas with pseudoalveolar formation (case 6ST). (C) Some tumors were composed predominantly of primitive round cells arranged in solid sheets or vague nests, with features of undifferentiated round cell sarcoma (5ST). Kidney tumors with BCOR-ITD show similar histologic features and are composed of undifferentiated round-to-ovoid cells with scant eosinophilic cytoplasm and vesicular nuclei: (E) case 7K; (F) case 5K. (G) Some tumors show predominantly small blue cell morphology with alternation of hypercellular and hypocellular areas (case 10K). All tumors show strong and diffuse nuclear expression of BCOR by immunohistochemistry: (D) case 10ST; (H) case 6K. The inset in panels (C), (E), and (F) shows images at a higher magnification. Scale bar: 100 μm.

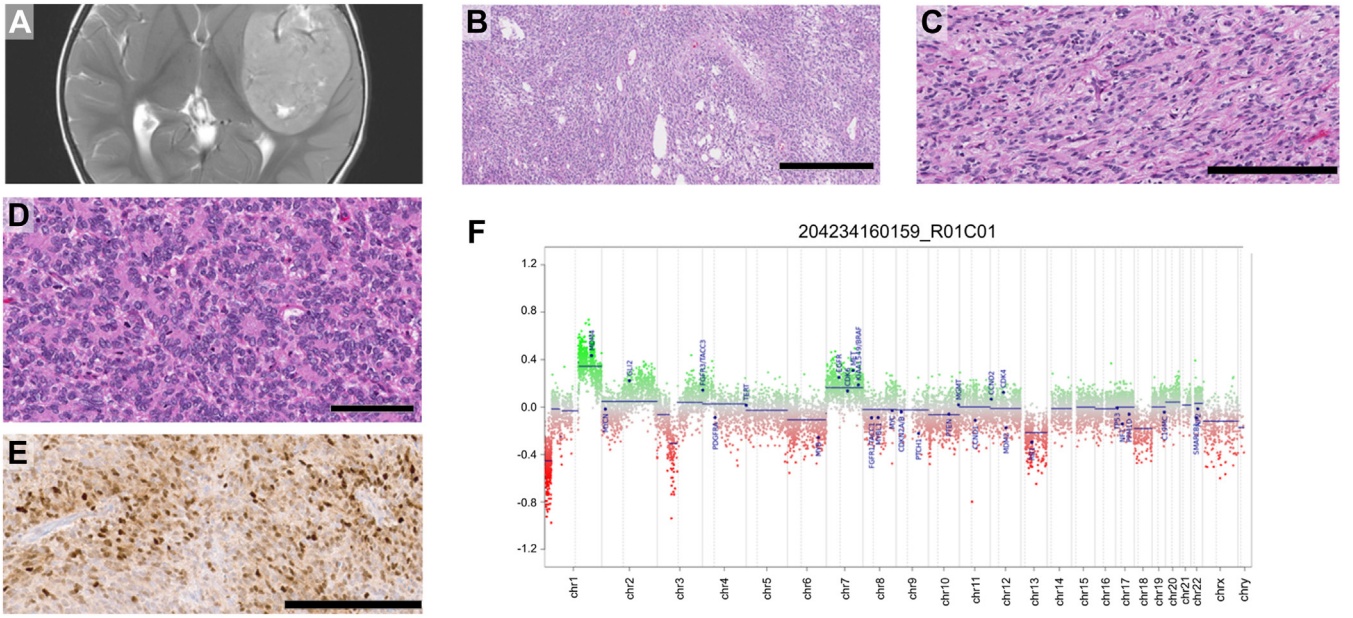

Figure 2.
Representative images of a high-grade neuroepithelial tumor [HG-NET] with BCL6-correpresor gene (*BCOR*) alterations: case 3N. (A) Computed tomography scan of the brain at diagnosis showing a large mass in the temporal lobe. (B) Histologic appearance of the primary tumor showing variably cellular neoplasm with some microcystic changes. (C) The tumor is composed of a combination of spindle-to-oval cells with fine chromatin and eosinophilic to clear cytoplasm. (D) The recurrent tumor shows areas with pseudorosettes in an ependymoma-like appearance. (E) Tumor cells showing nuclear expression of cyclin D1 by immunohistochemistry. (F) A copy number variation analysis of the recurrent tumor demonstrated multiple and complex chromosome gains and losses. Scale bars: (B) 150 μm; (C), (D), and (E) 200 μm.

with *BCOR* alterations," with optimal calibrated scores (>0.9). Of these cases, 16 matched to the subclass SBRCT-BCOR, irrespective of their location (12 PMMTI/UND and 4 CSSK), and 4 to the CCSK methylation family (1 PMMTI/UND and 3 CCSK). In the 2 PMMTI classified into the methylation class ESS-HG, a *YWHAE::NUTM2* rearrangement (9ST) and *BCOR-ITD* (16ST) were identified. The remaining 2 cases were also classified in the methylation class family "sarcoma with *BCOR* alterations" but with lower scores (0.77 in the methylation subclass SBRCT-BCOR for case 6K with *BCOR-ITD*, and 0.77 in the ESS-HG subclass for case 11ST with a *YWHAE::NUTM2* rearrangement).

Of interest, all PMMTI and CCSK cases without molecular confirmation were classified within the ESS-HG methylation family, with 3of the 6 cases with optimal calibrated scores (Table 2). The CCSK with negative results by RT-PCR was classified in the methylation class CCSK but with a suboptimal score (0.83), whereas the HG-NET without molecular confirmation matched to the HG-NET BCOR (score >0.9) according to the CNS tumor classifier (v11b4) (Table 2).

We further analyzed the samples by clustering analyses and compared them to a cohort of 26 the previously published HG-NET BCOR[13] and samples randomly extracted from internal and external data sets among those classified as mimics (EWS, EFT-CIC, ATRT, and rhabdoid tumor). An unsupervised hierarchical clustering analysis performed on the 1000 most variable probes of the whole-genome DNAm data showed 5 separated clusters (HG-NET BCOR, SOFT/CCSK BCOR, ATRT/Rhab, EFT-CIC, and EWS). *BCOR*-related tumors in the soft tissue and kidney clustered together, whereas they were clearly separated from CNS HG-NET, as evidenced by the MDS (Fig. 3).

Interestingly, the hierarchical clustering and heatmap of β values relative to the high-quality CpG islands (Fig. 4) confirmed the existence of separate clusters between HG-NET BCOR and ST/CCSK BCOR. *YWHAE::NUTM2*-rearranged tumors clustered together. Cases without molecular confirmation clustered in the ST/CCSK BCOR class (Supplementary Figs. S2 and S3), suggesting their possible grouping in the *BCOR*-family. The partial gain in chromosome 10q in 1 case (19ST), encompassing the *FAM22* and *NUTM2* loci, suggests possible rearrangements with activating pathways similar to those involved in *BCOR-ITD* malignancies, but this could not be confirmed because of technical issues.

Of note, 2 subclusters in *BCOR*-altered sarcomas were evident: the first one including older children (aged >1 year, with an average age of 5 years and range of 1-10 years), irrespective of tumor type, and the second one consisting of younger patients (aged <1 year, with an average age of 4 months and range of 0-11 months) (Supplementary Fig. S3).

Copy Number Variation Analysis and Survival

The CNV plots of all tumors are shown in Supplementary Figure S4. For those with evaluable CNV plots (32 samples), the analysis showed an almost flat profile in 19 cases (9/18 PMMTI/UND, 8/10 CCSK, and 2/4 HG-NET); 1q gain in 5 cases (2 PMMTI, 1 HG-NET, and 2 CCSK) associated with a loss of 9p (*CDKN2A/B*) in 2 cases (1 PMMTI and 1 CCSK); loss of 13q (*RB1* mapping) in 2 cases (1 HG-NET and 1 CCSK); and 10q loss (*PTEN* mapping) (1 PMMTI and 1 CCSK). The latter was found in another PMMTI (10ST). Finally, *CDK6* amplification was evident in 1 UND case.

CNVs were more often observed in relapsed tumors (Fig. 5A-D and Table 2). The Kaplan-Meier analysis showed that ≥2 alterations in CNV plotting significantly correlated with worse OS probability in the 20 patients for whom follow-up time was available. Indeed, the median OS was 24 months (95% CI, 1.382-20.88) in the CNV-altered group, whereas this was not reached (95% CI, 0.04790-0.7235) in the flat CNV group ($P = .0475$) (Fig. 5F).

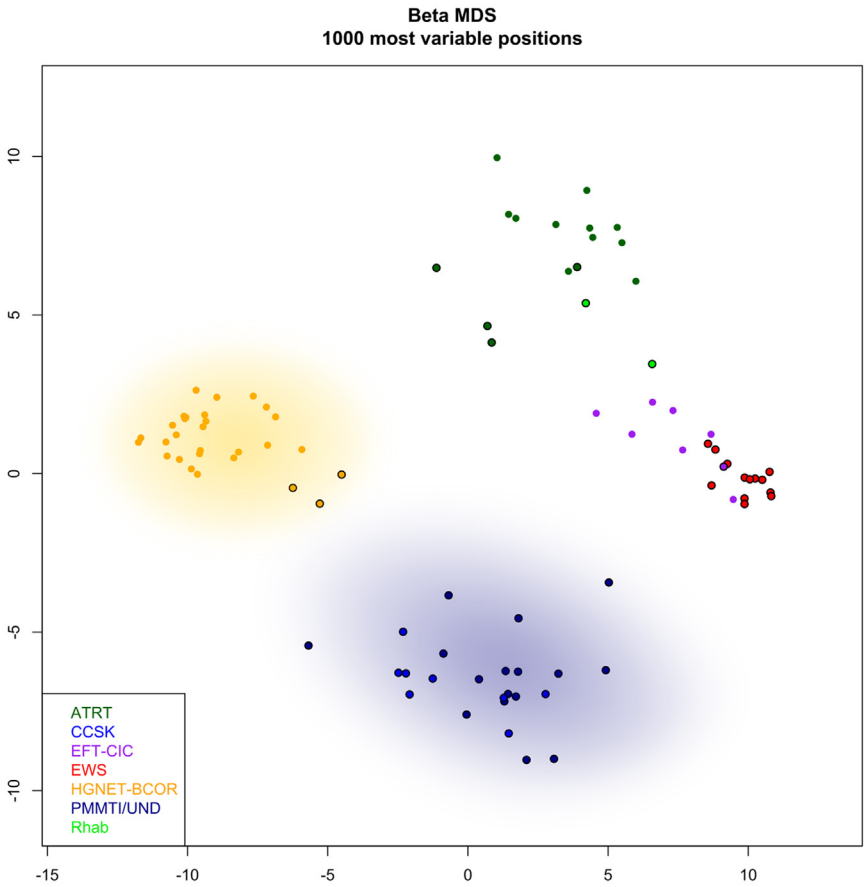

Figure 3.
The multidimensional scaling (MDS) analysis performed on the 1000 most variable probes of the whole-genome DNA methylation data shows a close similarity between soft tissue tumors (primitive myxoid mesenchymal tumors/undifferentiated sarcomas [PMMTI/UND]) and kidney tumors (clear cell sarcomas of the kidney [CCSK]) with BCL6-correpresor gene (*BCOR*) alterations (blue cloud) versus central nervous system tumors with *BCOR* alterations (yellow cloud). Color legend of the MDS plot is as follows: soft tissue tumor with *BCOR* alterations (PMMT/UND), dark blue; kidney tumors with *BCOR* alterations (CCSK), electric blue; central nervous system tumors with *BCOR* alterations (high-grade neuroepithelial tumors [HG-NET] BCOR), yellow; Ewing sarcoma (EWS), red; CIC-rearranged sarcoma (EFT-CIC), violet; atypical teratoid rhabdoid tumor (ATRT), dark green; and rhabdoid tumor (Rhab), light green. Bolded dots are internal cases.

In addition, the CNV analysis was able to show the rearrangement involving *YWAHE* for case 9ST associated with chromosome 10q gain (Fig. 6A, B), whereas *BCOR-ITD* was evident in 12 cases (Fig. 6C).

Differentially Methylated Regions

A functional enrichment analysis of DMRs in the 2 groups of BCOR-expressing soft tissue and kidney tumors (BCOR PMMTI/UND vs CCSK) failed to demonstrate significantly enriched pathways, confirming their close relationship (Supplementary Table S1). Looking at specific differentially methylated genes, we found 40 DMRs, all hypermethylated in CCSK. Five of these regions are located on chromosome 11 and include *WT1*, its antisense noncoding RNA *WT-AS1*, and *CFTR* gene regions.

In contrast, CNS tumors and sarcomas (the soft tissue and kidney) with *BCOR* alterations showed thousands of DMRs and significant enrichment for different pathways (false discovery rate < 0.05). Some of the dysregulated pathways support the hypothesis of different histogenesis and developmental programs (eg, aminoacyl-tRNA biosynthesis, fatty acid metabolism, axon guidance, and endocytosis). The detailed differences are summarized in Supplementary Table S2.

Discussion

The recent World Health Organization classification of CNS tumors has incorporated DNAm profiling in the diagnostic workup of brain tumors, recognizing a high methylation score according to the classifier as an “essential” diagnostic criterion alternative to or in combination with the identification of a driver alteration detected by the molecular analysis.[23]

Moreover, methylome profiling has revealed a high reliability in sarcomas defining specific clusters coherent with morphology and gene expression although it is still an object of investigation, especially for rare histotypes.[11]

In this study, we analyzed the methylation profile of 34 pediatric malignancies, 27 with molecularly confirmed *BCOR-ITD* or *YWHAE* fusions.

In the WHO classification of soft tissue tumors, *BCOR-ITD* sarcomas are included in the category of small round cell undifferentiated sarcomas with *BCOR* alterations, together with the larger group of *BCOR*-rearranged sarcomas, most frequently

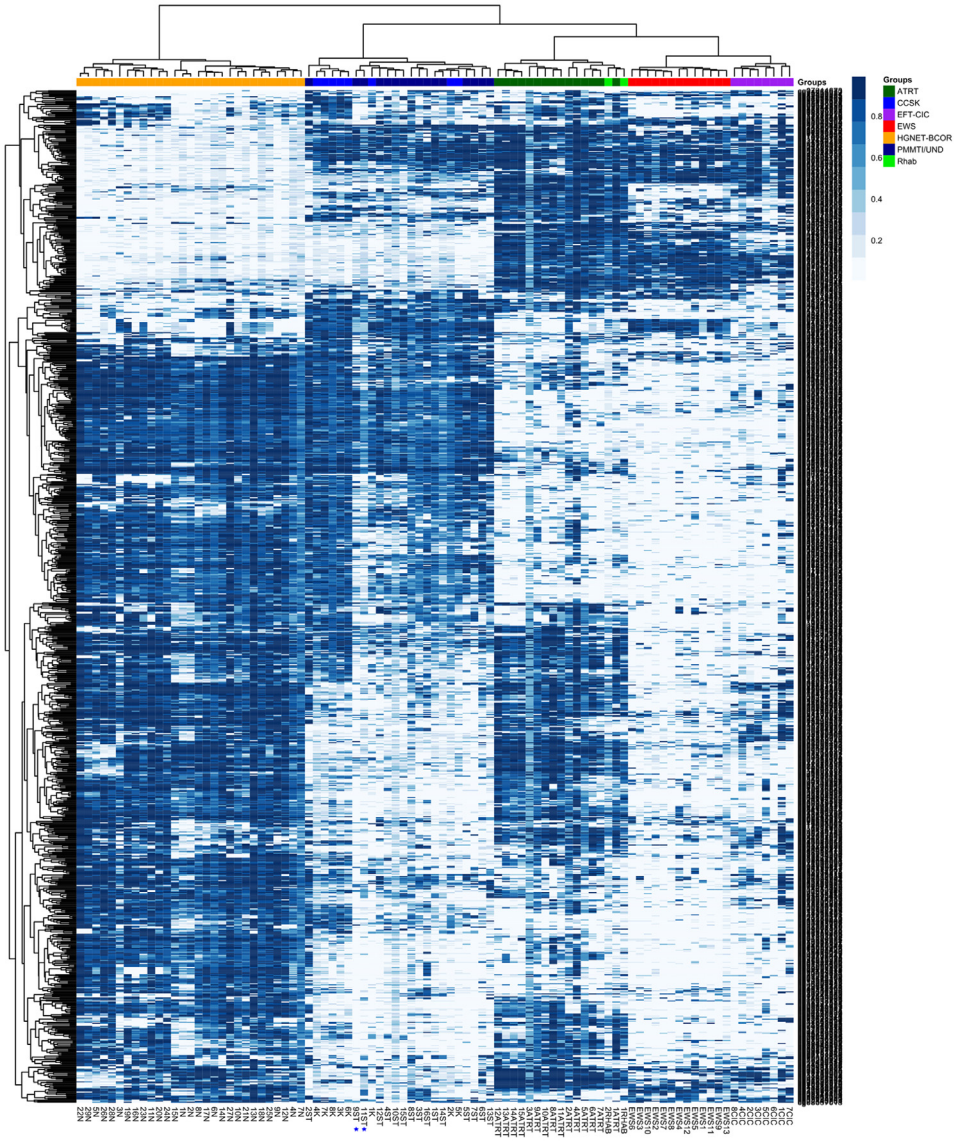

Figure 4.
Hierarchical clustering and heatmap of β values relative to the 1000 most variable probes of the whole-genome DNA methylation in the cohort. Clusters were obtained using the Ward minimum variance method using the Euclidean distance. Color legend: soft tissue tumor with BCL6-correpresor gene (*BCOR*) alterations (primitive myxoid mesenchymal tumors/undifferentiated sarcomas [PMMT/UND]), dark blue; kidney tumors with *BCOR* alterations (clear cell sarcomas of the kidney [CCSK]), electric blue; central nervous system tumors with *BCOR* alterations (high-grade neuroepithelial tumors [HG-NET] BCOR), yellow, Ewing sarcoma (EWS), red; CIC-rearranged sarcoma (EFT-CIC), violet; atypical teratoid rhabdoid tumor (ATRT), dark green; and rhabdoid tumor (Rhab), light green. Blue stars indicate *YWHAE::NUTM2* rearranged tumors.

characterized by *BCOR::CCNB3*, or by uncommon fusions such as *BCOR::MAML3*, *ZC3H7B::BCOR*, and *KMT2D::BCOR*, and other unknown fusion partners.[24]

Although previous studies have investigated the methylation profile of malignancies with *BCOR-ITD* (or alternative fusions)[13,25,26,27] including CCSK, HG-NET, and HG-ESS, only a few have analyzed PMMTI/UND so far. To the best of our knowledge, this series of pediatric *BCOR-ITD* malignancies includes the largest number of PMMTI/UND investigated by methylation profiling.

Our study supports the role of methylation profiling as a putative diagnostic tool in pediatric *BCOR*-related tumors. In fact, all PMMTI/UND and CCSK with molecularly confirmed *BCOR-ITD* were identified according to the classifier in the methylation class family sarcoma with *BCOR* alteration, with good to optimal calibrated scores, except for 1 case (11ST) with a borderline calibrated score probably related to a high content of inflammatory cells, as previously reported by Koelsche et al.[11]

Of interest, the only 2 UNDs with *YWHAE::NUTM2* fusion were classified in the methylation class of ESS-HG. Moreover, this category encompassed 5 of the 6 tumors without molecular confirmation.

DNAm is considered the fingerprint of the cell lineage from which the tumor may have originated, making it useful for a molecular classification based on the cell of origin. Thus, it is not surprising that HG-NET and extracranial-*BCOR-ITD* sarcomas formed a single common clade of *BCOR*- rearranged tumors, whereas they clearly formed 2 distinct subclusters with HG-ESS and sarcoma with BCOR alteration were very close and almost overlapped.

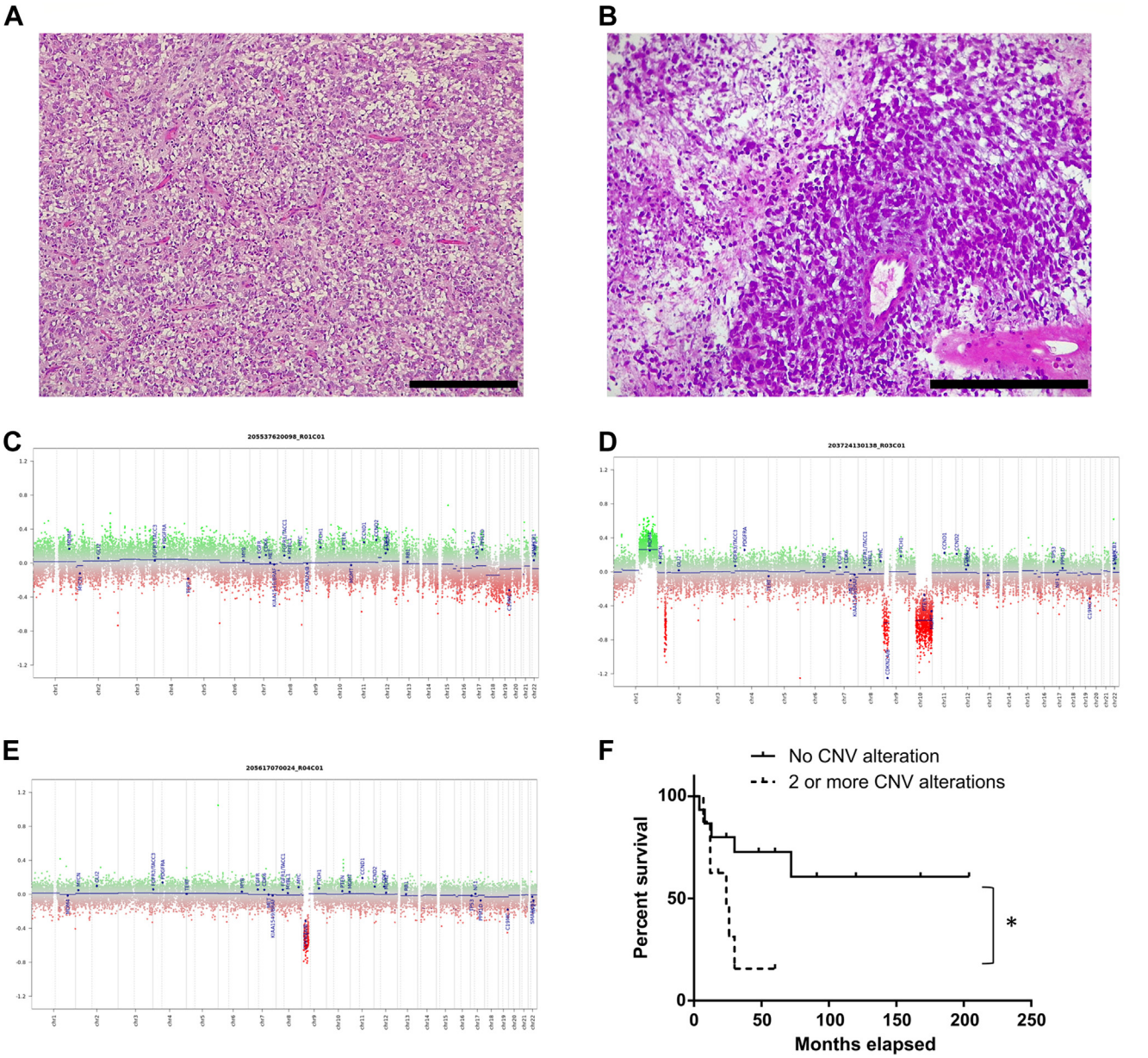

Figure 5.
Histologic appearance of a primary paraspinal/gluteal soft tissue tumor (14ST) (A) and recurrent tumor 10 years later (2ST) (B) from the same patient. (C, D) Copy number variation (CNV) changes detected in the respective tumors as in (A, B): the primary tumor (C) with no significant CNV, and the recurrent tumor (D) showing 1q gain, 9p loss (*CDKN2A/B*) and 10q loss (*PTEN*). (E) CNV plot showing 9p loss (*CDKN2A/B*) in a 4-year-old patient with confirmed *BCOR*-ITD tumor (16ST) but classifying in the endometrial stromal sarcoma (high grade) methylation class. (F) CNV and its correlation with survival of patients with BCL6-correpresor gene sarcoma. Kaplan-Meier analysis for overall survival in 20 patients with ST (11) and clear cell sarcomas of the kidney (9) with available follow-up information, stratified by CNV (0-1 vs $\geq$2 alterations), respectively. Differences between groups were compared with the log-rank test ($P = .0475$). Scale bars: (A) 150 μm; (B) 200 μm.

A similar situation has been described for *DICER*-mutated tumors arising inside[28] or outside the CNS[29] and for intracranial angiomatoid fibrous histiocytoma–like neoplasms[30] with *FET-CREB* fusions[31] versus their counterparts in soft tissues.[32] Possibly, the same driving genetic alteration occurring in different stem cells plays equivalent functional effects (ie, determines the differentiation arrest). This possibility is supported by our collected data showing, in the CNS tumors, significant differences in methylation with enrichment in pathways, suggesting divergent tissue differentiation and functions compared with those of the soft tissue tumors. Conversely, CCSK and *BCOR*-related soft tissue sarcomas cluster together with only a few significantly differentially methylated genes. The methylation of early developmental genes (eg, *WT1* and *CFTR*) supports the hypothesis of a more differentiated cell of origin in the CSSK, compared with the soft tissue tumors with *BCOR* alterations, and is in agreement with the fact that CCSK usually occur in older patients.

Clustering of sarcoma with *YWHAE::NUTM2* in the HG-ESS methylation class further supports the close relationship among all extracranial *BCOR*-altered malignancies and their distinction from HG-NET. However, it deserves further investigation to understand whether it might be indicative of

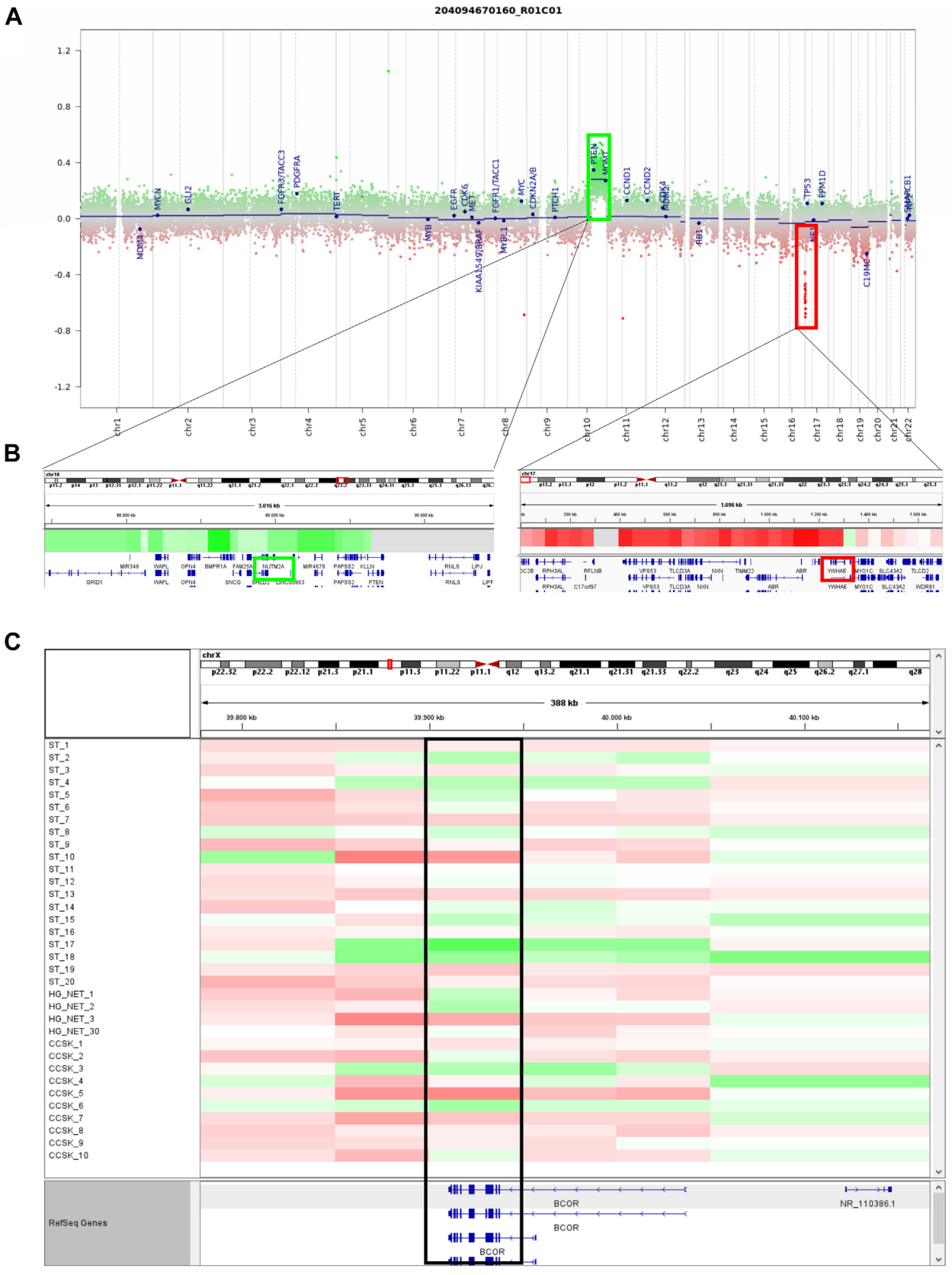

Figure 6.
(A) Copy number variation plot for case 9ST showing the structural rearrangement in chromosomes 10q and 17p (*YWHAE::NUTM2A* fusion). (B) Integrative genomic viewer (IGV) snapshot detailing the gene mapping in the indicated regions. Boxes highlight *NUTM2A* on chromosome 10 (green) and *YWHAE* on chromosome 17p (red). (C) IGV snapshot detailing the copy number data and mapping of BCL6-correpresor gene (*BCOR*) in all samples analyzed. A red-to-green scale corresponds to copy numbers from −1 to 1 log2 (ratio) with respect to normal controls. Both deletions and amplifications can have continuous valued numbers represented by shading. The red box highlights the exon mapping. Green samples show possible expression of *BCOR-ITD*.

distinctive biological features or simply reflects the activation of site and age-related patterns. In our view, although not molecularly confirmed, the clustering of 5 tumors with morphologic features of PMMTI/UND support their categorization as *BCOR-ITD* sarcomas, together with the immunophenotype in particular, the strong expression of BCOR and cyclin D1, as emphasized by Koelsche et al[11] in their study of validation of sarcoma classifier, based on morphology-methylation integration. Thus, methylation profiling may be contributive and add significant information in cases in which RNA is insufficient or poorly preserved. The series of 33 pediatric and adult *BCOR-ITD* malignancies recently reported by Bouchoucha et al[25] is in agreement with this study. A DNAm analysis, performed on 21 *BCOR-ITD* tumors, including brain tumors (10), with 4 HG-ESS, 10 URCSs, and 2 bone tumors, demonstrated that these malignancies were consistently segregated into 2 separate but close groups, a finding confirmed also by transcriptome. By the comparison of gene signatures with single-cell RNA-Seq atlases, the study highlights the close relationship of HG-NET and *BCOR-ITD* sarcomas/CCSK/HG-ESS with neural and mesenchymal cells in keeping with different cells of origin.

Despite the shared methylation classes and morphologic similarity, CCSK and PMMTI/UND differ in their clinical manifestations and behavior. PMMTI/UND arise in the first year of life and have a highly aggressive behavior. In contrast, the mean age of CCSK occurrence is about 2 years and the patients have a better outcome. In the recent series reported by Bouchoucha et al,[25] 6 of the 7 patients affected by CCSK were alive, in line with the survival of 7 of the 9 in this study.

Although most of the CCSK cases analyzed showed an almost flat CNV profile, in line with the previously described limited chromosomal changes in CCSK by a comparative genomic hybridization analysis,[33] a multivariate analysis could not be performed because of the limited number of cases. However, it is hypothesized that a flat CNV may contribute to the more favorable prognosis in CCSK compared with that of the soft tissue tumors in our current series.

Interestingly, $\geq$2 CNV alterations were significantly associated with a worse OS in general in extracranial *BCOR-ITD* malignancies. The most frequent CNV involved 1q gain and losses at loci of tumor suppressor genes (*PTEN* and *CDKN2A*/*B*), suggesting that these alterations may play a role in the aggressive clinical behavior of *BCOR*-altered malignancies.

In summary, in this study, methylation profiling correlated with the presence of *BCOR-ITD* or *YWHAE::NUTM2* molecularly detected, confirming its role as a diagnostic tool. Moreover, our data further corroborate the hypothesis that CCSK and PMMTI/UND represent 2 closely related entities, although a greater number of cases are needed to better define the biological basis of clinical differences between these 2 groups. The potential role of a cumulative effect of CNV or the combination of selective recurrent alterations in the aggressive clinical behavior of PMMTI/UND is a promising field of investigation.

Acknowledgments

The authors thank all patients and their families; Claudia Nardini for the methylation analysis and Carmen D'Amore for the statistical analysis revision; and "Il cuore grande di Flavio," "Il sorriso di Costanza," "Fondazione Heal," and Banca IFIS for their support.

Author Contributions

E.M. and R.A. performed study concept and design; C.M.S, A.C., F.D.C., L.P., A.Z., and E.M. performed acquisition, analysis, and interpretation of data and statistical analyses; G.M.M., A.S., A.D.G., A.M., A.G., G.B., and A.F. collected tumor samples and clinical data; C.M.S., R.A., and E.M. drafted the original manuscript; M.T., M.R.-M., and F.L. reviewed and revised the paper. All authors read and approved the final version of the paper.

Data Availability

All data/information are available in the manuscript and in the supplementary material. The data sets used and analyzed in this study are available from the corresponding authors upon a reasonable request.

Funding

This research was supported by the Italian Ministry of Health, Ricerca Corrente (202005_ONCO_MIELE to E.M; 202005_ONCO_ALAGGIO to R.A., and 202203_FBG_MILANO.1.15 to G.M.M) and partly by the Marjory K. Harmer Endowment for Pediatric Pathology Research (to M.R.-M.).

Declaration of Competing Interest

None reported.

Ethics Approval and Consent to Participate

This study was reviewed and approved by Bambino Gesù Children's Hospital Ethical Committee (protocol number 2126_OPBG_2020, June 17, 2020; final approval received on November 22, 2020) and by the University of Pittsburgh (STUDY19080192; final approval received on February 25, 2020), in compliance with the ethics principles of the Declaration of Helsinki.

Supplementary Material

The online version contains supplementary material available at https://doi.org/10.1016/j.modpat.2022.100039

References

1. Astolfi A, Fiore M, Melchionda F, Indio V, Bertuccio SN, Pession A. BCOR involvement in cancer. *Epigenomics*. 2019;11(7):835–855.
2. Wang Z, Gearhart MD, Lee YW, et al. A non-canonical BCOR-PRC1.1 complex represses differentiation programs in human ESCs. *Cell Stem Cell*. 2018;22(2):235–251.e9.
3. Ueno-Yokohata H, Okita H, Nakasato K, et al. Consistent in-frame internal tandem duplications of BCOR characterize clear cell sarcoma of the kidney. *Nat Genet*. 2015;47(8):861–863.
4. Kao YC, Sung YS, Zhang L, et al. Recurrent BCOR internal tandem duplication and YWHAE-NUTM2B fusions in soft tissue undifferentiated round cell sarcoma of infancy: overlapping genetic features with clear cell sarcoma of kidney. *Am J Surg Pathol*. 2016;40(8):1009–1020.
5. Sturm D, Orr BA, Toprak UH, et al. New brain tumor entities emerge from molecular classification of CNS-PNETs. *Cell*. 2016;164(5):1060–1072.
6. Mariño-Enriquez A, Lauria A, Przybyl J, et al. BCOR internal tandem duplication in high-grade uterine sarcomas. *Am J Surg Pathol*. 2018;42(3):335–341.
7. Clark SJ, Melki J. DNA methylation and gene silencing in cancer: which is the guilty party? *Oncogene*. 2002;21(35):5380–5387.

8. Capper D, Stichel D, Sahm F, et al. Practical implementation of DNA methylation and copy-number-based CNS tumor diagnostics: the Heidelberg experience. *Acta Neuropathol*. 2018;136(2):181–210.
9. Renner M, Wolf T, Meyer H, et al. Integrative DNA methylation and gene expression analysis in high-grade soft tissue sarcomas. *Genome Biol*. 2013;14(12):r137.
10. Koelsche C, Hartmann W, Schrimpf D, et al. Array-based DNA-methylation profiling in sarcomas with small blue round cell histology provides valuable diagnostic information. *Mod Pathol*. 2018;31(8):1246–1256.
11. Koelsche C, Schrimpf D, Stichel D, et al. Sarcoma classification by DNA methylation profiling. *Nat Commun*. 2021;12(1):498.
12. Antonescu CR, Kao YC, Xu B, et al. Undifferentiated round cell sarcoma with BCOR internal tandem duplications (ITD) or YWHAE fusions: a clinicopathologic and molecular study. *Mod Pathol*. 2020;33(9):1669–1677.
13. Capper D, Jones DTW, Sill M, et al. DNA methylation-based classification of central nervous system tumours. *Nature*. 2018;555(7697):469–474.
14. Petruzzellis G, Alessi I, Colafati GS, et al. Role of DNA methylation profile in diagnosing astroblastoma: a case report and literature review. *Front Genet*. 2019;10:391.
15. Miele E, De Vito R, Ciolfi A, et al. DNA methylation profiling for diagnosing undifferentiated sarcoma with capicua transcriptional receptor (CIC) alterations. *Int J Mol Sci*. 2020;21(5):1818.
16. Morris TJ, Butcher LM, Feber A, et al. ChAMP: 450k chip analysis methylation pipeline. *Bioinformatics*. 2014;30(3):428–430.
17. Murtagh F, Legendre P. Ward's hierarchical agglomerative clustering method: which algorithms implement WARD's criterion? *J Classif*. 2014;31(3):274–295.
18. Suzuki R, Shimodaira H. Pvclust: an R package for assessing the uncertainty in hierarchical clustering. *Bioinformatics*. 2006;22(12):1540–1542.
19. Phipson B, Maksimovic J, Oshlack A. missMethyl: an R package for analyzing data from Illumina's HumanMethylation450 platform. *Bioinformatics*. 2016;32(2):286–288.
20. Alaggio R, Ninfo V, Rosolen A, Coffin CM. Primitive myxoid mesenchymal tumor of infancy: a clinicopathologic report of 6 cases. *Am J Surg Pathol*. 2006;30(3):388–394.
21. De Lima L, Sürme MB, Gessi M, et al. Central nervous system high-grade neuroepithelial tumor with BCOR alteration (CNS HGNET-BCOR)-case-based reviews. *Childs Nerv Syst*. 2020;36(8):1589–1599.
22. Magro G, Salvatorelli L, Alaggio R, et al. Diagnostic utility of cyclin D1 in the diagnosis of small round blue cell tumors in children and adolescents. *Hum Pathol*. 2017;60:58–65.
23. Louis DN, Perry A, Wesseling P, et al. The 2021 WHO Classification of Tumors of the central nervous system: a summary. *Neuro Oncol*. 2021;23(8):1231–1251.
24. Carter CS, Patel RM. Important recently characterized non-Ewing small round cell tumors. *Surg Pathol Clin*. 2019;12(1):191–215.
25. Bouchoucha Y, Tauziède-Espariat A, Gauthier A, et al. Intra- and extra-cranial BCOR-ITD tumours are separate entities within the BCOR-rearranged family. *J Pathol Clin Res*. 2022;8(3):217–232.
26. Kommoss FKF, Stichel D, Schrimpf D, et al. DNA methylation-based profiling of uterine neoplasms: a novel tool to improve gynecologic cancer diagnostics. *J Cancer Res Clin Oncol*. 2020;146(1):97–104.
27. Specht K, Zhang L, Sung YS, et al. Novel BCOR-MAML3 and ZC3H7B-BCOR gene fusions in undifferentiated small blue round cell sarcomas. *Am J Surg Pathol*. 2016;40(4):433–442.
28. Kamihara J, Paulson V, Breen MA, et al. DICER1-associated central nervous system sarcoma in children: comprehensive clinicopathologic and genetic analysis of a newly described rare tumor. *Mod Pathol*. 2020;33(10):1910–1921.
29. Kommoss FKF, Stichel D, Mora J, et al. Clinicopathologic and molecular analysis of embryonal rhabdomyosarcoma of the genitourinary tract: evidence for a distinct DICER1-associated subgroup. *Mod Pathol*. 2021;34(8):1558–1569.
30. Kao YC, Sung YS, Zhang L, et al. EWSR1 fusions with CREB family transcription factors define a novel myxoid mesenchymal tumor with predilection for intracranial location. *Am J Surg Pathol*. 2017;41(4):482–490.
31. Sloan EA, Chiang J, Villanueva-Meyer JE, et al. Intracranial mesenchymal tumor with FET-CREB fusion-A unifying diagnosis for the spectrum of intracranial myxoid mesenchymal tumors and angiomatoid fibrous histiocytoma-like neoplasms. *Brain Pathol*. 2021;31(4), e12918.
32. Rossi S, Szuhai K, Ijszenga M, et al. EWSR1-CREB1 and EWSR1-ATF1 fusion genes in angiomatoid fibrous histiocytoma. *Clin Cancer Res*. 2007;13(24):7322–7328.
33. Barnard M, Bayani J, Grant R, Zielenska M, Squire J, Thorner P. Comparative genomic hybridization analysis of clear cell sarcoma of the kidney. *Med Pediatr Oncol*. 2000;34(2):113–116.